Chapter 6: Discussion

6.1 Introduction

This chapter discusses the results of the centrifuge tests described in chapter 5 in relation to the verification of the hypothesis of pile failure proposed in chapter 3 (section 3.5). The failure of the piles in the model centrifuge tests has been compared with the observed pile failure in the field case histories. This chapter also links the correlations obtained from the study of case histories with a theory of pile failure backed up by the centrifuge test results. A parallel has also been drawn between Euler's classical buckling and pile buckling.

In the analytical work described in this chapter, an attempt has been made to back-analyse the results of the centrifuge tests described in chapter 5.

6.2 Verification of the proposed pile failure hypothesis

As mentioned earlier, one of the aims of this research is to verify the hypothesis of pile failure by buckling instability set out in section 3.5. It immediately becomes obvious from Table 5.2 that the piles having a P/P_{cr} ratio close to 1 failed. The loads in the piles marked 7, 8 and 10 were purely axial. The pile heads were restrained in the direction of shaking (no inertia effects) and the piles buckled transversely to the direction of shaking, Figures 5.14(a), 5.15(a) and 5.26(b). It must also be remembered that the piles were carrying the same load (the load at which they later failed) at 50-g and were stable before the earthquake. The stress in the pile section is well within the elastic range of the material (less than 30% of the yield strength) but it failed as the earthquake was fired. This confirms that the support offered by the soil was eliminated by earthquake liquefaction and that the pile started to buckle in the direction of least elastic bending stiffness. Thus it may be concluded that, if the axial load is high enough ($P/P_{cr} \geq 1$) it may not be necessary to invoke lateral spreading of the soil to cause a pile to collapse and piles can collapse before lateral spreading starts once the surrounding soil has liquefied.

6.3 Replication of observed pile failure in centrifuge tests

Figure 5.7 shows the surface observation of the piles after test SB-02. A similar form of failure was also observed for pile 12 in test SB-06, Figure 5.33. These piles were not restrained at the top and therefore could experience any inertia load communicated to the head mass. It may be noted that the heads of the piles duly rotated and translated. This is quite similar to visual observations of the collapsed piled structures in laterally spreading soil shown in Figures 1.2(c), 6.1(a). The building shown in Figure 6.1(a) is Kandla port tower in laterally spreading soil, which tilted by 15 degrees after the 2001 Bhuj earthquake (India).

Figure 6.1 (c) shows the point of hinge formation in the failure of a three-storey R.C building revealed after excavation following the 1995 Kobe earthquake. As shown in Figures 5.14(a), 5.15(a) in chapter 5, and Figure 6.1(b) the piles that failed during the earthquake in the centrifuges tests had hinges form in the top third of the pile. There is a similarity between the locations of hinge formation in the centrifuge test and in the aftermath of real earthquakes.

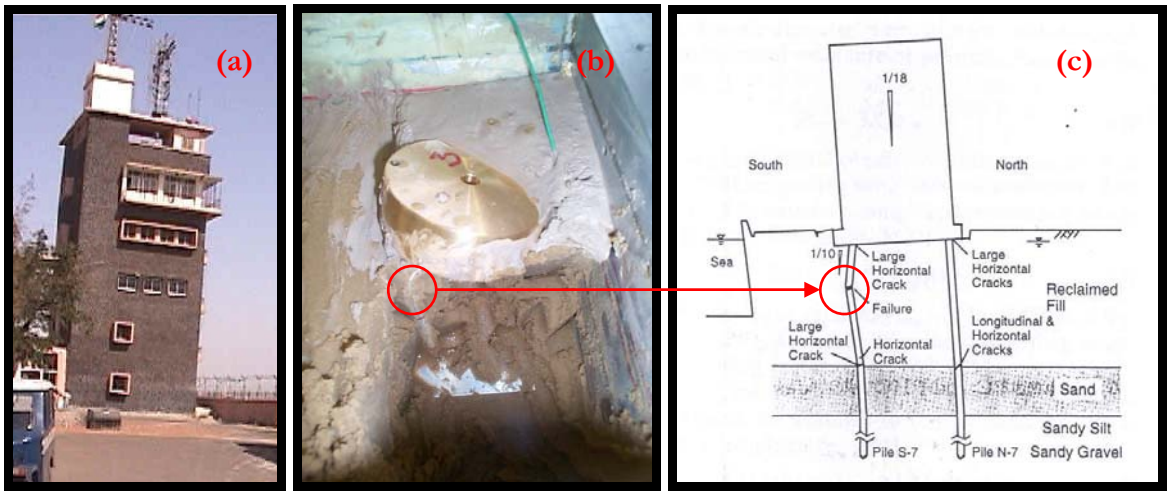

Figure 6.1: (a): Observed failure of a piled foundation (Kandla Port tower) in 2001 Bhuj earthquake, Madabhushi et al. (2001);. (b): Pile (marked 3) failure in centrifuge test SB-02; (c): Excavated piles in a 3 storied building in 1995 Kobe earthquake, Tokimatsu et al., (1997).

This demonstrates that the pile failure mechanisms observed in the field can be reproduced in a scaled model using dynamic centrifuge modelling. It must be noted that the real piled buildings were in laterally spreading soil whereas the model piles in the experiments were in level ground. Thus the centrifuge tests point out that piles can fail in level ground under the action of axial load and lateral inertia load. It is not necessary to invoke lateral spreading of the soil to cause a pile to fail.

After the detailed investigation of the failure of piles during 1995 Kobe earthquake, Tokimatsu and Asaka (1998) report that:

"*In the liquefied level ground, most PC piles (Prestressed Concrete pile used before 1980's) and PHC piles (Prestressed High Strength Concrete piles used after 1980's) bearing on firm strata below liquefied layers suffered severe damage accompanied by settlement and/or tilting of their superstructure, …..*".

This shows that the centrifuge test results are in good agreement with field observations.

6.4 Buckling of piles as soil liquefies

As mentioned in chapter 2, buckling of piles is currently considered in design under the following headings:

1. During installation by driving, especially of an unsupported pile.
2. Partially exposed piles as in jetties or offshore platforms.
3. Piles in very soft clay.

The key conclusion from the centrifuge tests is that fully embedded end-bearing piles passing through saturated, loose to medium dense sands and resting on a hard layer can buckle under the action of axial load alone if the surrounding soil liquefies in an earthquake. The stress in the pile section will initially be within the elastic range and the buckling length will be the entire length of pile in liquefied soil.

Lateral loading, due to slope movement (lateral spreading), inertia, or out-of-straightness, will increase lateral deflections which in turn can cause plastic hinges to form, reducing the buckling load, and promoting more rapid collapse. These lateral load effects are, however, secondary to the basic requirements that piles in liquefiable soils must be checked against Euler's buckling. This is the basic requirement for the proposed design method of piled foundations discussed in chapter 7.

The critical load (P_{cr}) of an axially loaded structure is defined as the minimum axial load at which the structure becomes unstable and the transverse deflection becomes indefinitely large. Stability analysis of elastic columns (see Timoshenko and Gere, 1961) shows that the lateral deflections caused by lateral loads are greatly amplified in the presence of axial loads. If δ_0 is the deflection of a cantilever column due to lateral loads alone, the final deflection (δ) gets amplified in the presence of axial load (P) following equation 6.1

$$\delta = \delta_0 \frac{1}{\left(1 - \frac{P}{P_{cr}}\right)} \tag{6.1}$$

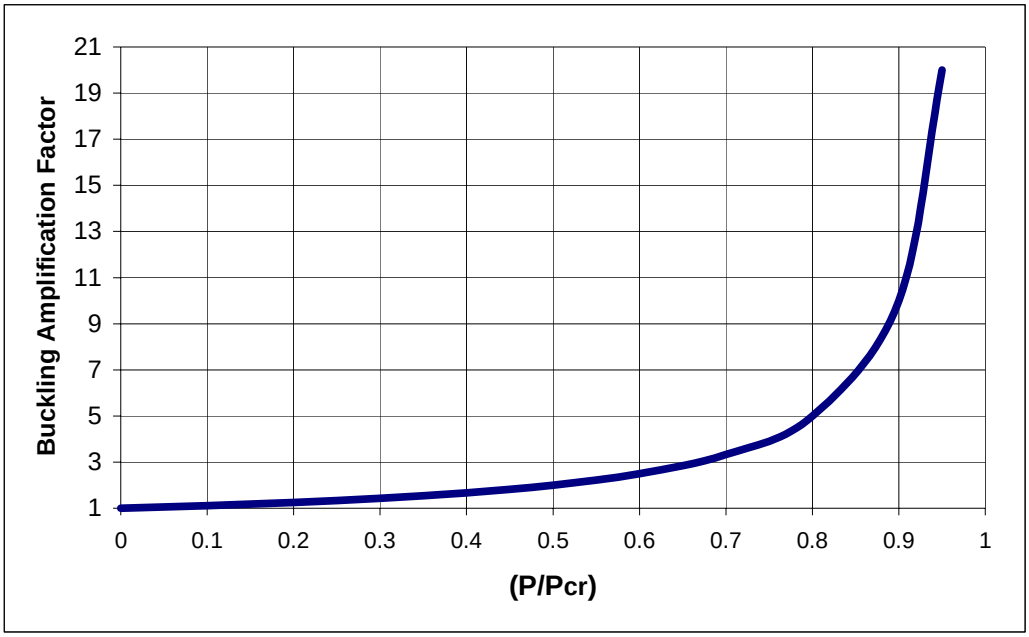

Figure 6.2: Buckling amplification factor versus normalised axial load.

The term (δ/δ_0) can be termed as "Buckling amplification factor (BAF)" given by equation 6.2

$$B.A.F = \frac{1}{\left(1-\frac{P}{P_{cr}}\right)} \tag{6.2}$$

This form of expression, sketched in Figure 6.2, can be used with good accuracy (less than 2% error) for all beam-columns having (P/P_{cr}) less than 0.6, Timoshenko and Gere (1961). Beyond the ratio of 0.6 the induced plastic strains cause a deterioration of elastic bending stiffness leading to a reduction in the critical buckling load P_{cr}, and to premature collapse.

From Figure 6.2, it is evident that the transverse deflection due to lateral load will be amplified at least 4 times for an axially loaded column (P/P_{cr}) more than 0.75. This lateral deflection will give rise to additional (P-δ) moment eventually leading to plastic collapse. This is consistent with the centrifuge test results where the piles having (P/P_{cr}) ratio above 0.75 failed under the combined action of axial and inertia. It is worth mentioning here that in spite of large inertia forces being applied in test SB-03, the piles having (P/P_{cr}) ratio less than 0.5 did not collapse.

It may be concluded that unless the (P/P_{cr}) ratio is high enough, lateral loads - however large they may be - cannot cause instability to a piled structure. However, the structure may collapse by

forming a plastic collapse mechanism i.e. failure by yielding of the material. This conclusion is also in good agreement with the study of case histories.

Table 6.1 reassembles 6 case histories of good performance of piled foundation studied in chapter 3 emphasising the (P/P_{cr}) ratio and information on lateral spreading.

Table 6.1: Good performance of piled foundations

Case History and Reference*	**(P/P_{cr})**	**Performance**	**Lateral spreading?**
10 storey-Hokuriku building [1]	0.06	Good	Yes, nearby ground moved by 2m
Landing bridge [2]	0.0045	Good	Yes, ground cracked and sand ejected
14 storey building [3]	0.006	Good	Yes, quay walls on the west, south and east moved.
Hanshin expressway pier [4]	0.05	Good	Yes, ground moved by 0.62m
LPG tank 101 [5]	0.05	Good	Yes, ground moved by 0.7m
Kobe Shimim hospital [6]	0.03	Good	No, ground subsided.

The number in the parenthesis refers to the serial number of the case history in Table 3.4 in chapter 3.

It must particularly be noted that five out of the six piled structures that performed well were in laterally spreading soil. They had a very low (P/P_{cr}) ratio and thus the pile deflections due to the lateral spreading loads were not amplified. It will be shown in Chapter 7 that a slenderness ratio below 50 signifies (P/P_{cr}) below 0.35 for steel and 0.15 for concrete. Thus it becomes obvious why piles in laterally spreading soil having slenderness ratio below 50 did not collapse. A contrasting behaviour of two piled tanks at the same site is discussed in 6.4.1.

6.4.1 Concept of critical depth for buckle initiation

It has been observed through the analysis of pore pressure data in all the centrifuge tests, for example Figure 5.18, that as shaking starts the pore pressure rises in the soil starting from the top and proceeding downwards and at the same time, the front of zero effective stress continues to advance swiftly downwards. It has been hypothesised that, with the advancement of this front, the pile will gradually be unsupported by the soil grains in a progressive fashion, top-down. When this advancing front reached a critical depth H_c given by equation 6.3, the pile would have

become elastically unstable following equation 3.1, taking $L_{eff} = 2\ H_c$ for a pile with no restraint at the head.

$$H_c = \sqrt{\frac{\pi^2 EI}{4P}} \tag{6.3}$$

This instability will cause the pile to begin to move slowly sideways in the direction of least elastic bending stiffness, thereby pushing the initially liquefied soil. This hypothesis has been verified by analysing the LVDT record and the pore pressure records surrounding pile 10 in test SB-06 described in section 5.3.2 and Figure 5.21.

The above concept of critical depth can be validated using the case histories of the piled tanks 101 and 106 (case history 6 and 15 respectively) described in Chapter 3. This particular example is chosen, as the two tanks were located in the same site (Figure 3.21a) and behaved differently; one collapsed and the other survived. The critical depth H_C, i.e. the depth of the front of zero effective stress, such that the structure first becomes unstable and buckles, will be estimated for this type of structure. Figure 6.3 shows the schematic representation of the tank structure.

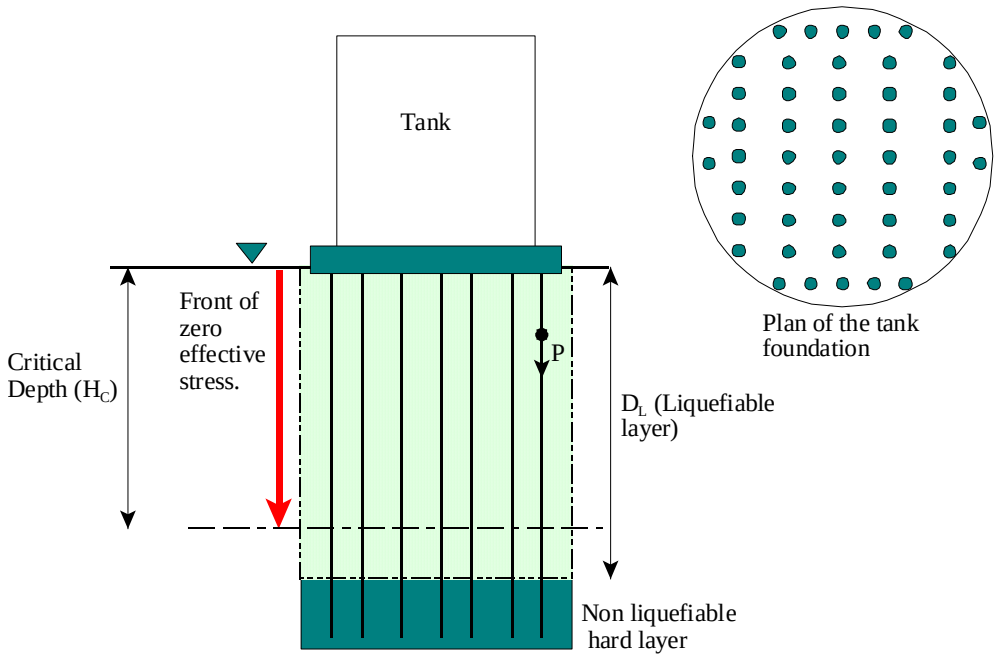

Figure 6.3: Schematic diagram showing the concept of "Critical Depth".

Let P be the axial load acting on each pile beneath the piled tank shown in Figure 6.3. It will be assumed that each pile is equally loaded. For a pile fixed at the tip and fixed in direction but free to translate at the top, the effective length (L_{eff}) is the unsupported length H_C, Figure 3.6. Earthquakes being dynamic events, considering the effect of lateral loads, it is reasonable to

adopt a safety factor of at least 2 against critical load to ensure stability of the structure, following Figure 6.2. This gives us a design value of H_C, equation 6.4.

$P = 0.5P_{cr} = 0.5\frac{\pi^2 EI}{H_c^2}$ which leads to

$$H_c = \sqrt{\frac{4.93EI}{P}} \tag{6.4}$$

The difference between equations 6.3 and 6.4 is due both to the different boundary conditions of the pile and that the effect of lateral load is considered only in equation 6.4. Table 6.2 estimates the critical depth for the tank foundations.

Table 6.2: Estimation of critical depth

Case history	**EI of the Pile section**	**P**	**H_C (Equation 6.4)**	**D_L Depth of liquefiable layer**	**Remarks**	**P_{cr}**	**P/P_{cr}**
LPG Tank 101, Kobe earthquake.	1.79×10^9N.m^2 1.1m dia RCC	4.1MN	46.4m	15m	Ground moved by 0.7m, good performance	79MN	0.05
LPG Tank 106, Kobe earthquake.	11.15×10^6N.m^2 0.3m dia RCC hollow	0.46MN	10.93m	15m	Ground moved and subsided, poor performance	0.38MN	1.2

It can be concluded that the piled structure becomes unstable for $H_C<D_L$, where D_L is the depth of liquefiable layer. It must be noted that the critical depth concept is a by-product of L_{eff} but it is particularly fruitful from practical point of view to evaluate the safety of existing piled foundations prone to axial instability.

6.5 "Euler's classical buckling" and "Pile buckling"

Test SB-04 was repeated as SB-05 (Table 4.3 and 4.12) but without soil where the model piles acted as cantilever struts. Figure 5.14(a&b) and 5.14(c) compare the mode shape of pile 7 in the two tests. For Euler's buckling, it is obvious that the hinge should form at the bottom for a cantilever strut (Figure 3.1, 1-g test) but for pile buckling it is observed that hinges form within the top half of the pile. It can also be observed that there is some plastic deformation below the point of hinge formation in the case of pile buckling.

Curvature being related to bending moment, the tests suggest that the deeper part of the "liquefied" soil zone offered resistance to the buckling pile and reduced bending moments in the lower half of its length. We might conclude that "liquefied" soil cannot prevent the initiation of buckling in an initially straight pile, but that some secondary support then becomes available.

It is evident that the resistance of the liquefied soil prevents the development of the full height buckle observed when a similar pile is tested in air. It will be demonstrated in subsequent sections that the difference in mode shape is due to the post-buckling behaviour of the pile. Unlike, Euler's classical buckling, pile buckling will involve the analysis in a resistive medium. Further details of the analysis are discussed in Section 6.9.

6.6 Resistance of liquefied soil

From the time history of LVDT records (Figure 5.26) in test SB-06, it is evident that the velocity of the pile head decreased in the process of progressive buckling through the resistive liquefied soil. In other words, the pile had a negative acceleration due to the resistance of the liquefied soil. The resistance increased tremendously after a certain amount of pile displacement (30% reference strain) as can be observed from the pressure cells readings, Figure 5.28.

Experimental work has been carried out by Takahashi et al (2002) to study the lateral resistance of piles in a liquefied soil having realistic over burden pressure. A pile was modelled as a buried cylinder that could be pushed laterally through a liquefied soil, Figure 6.4. The displacement rate of the cylinder varied from 1mm/s to 100mm/s. The test results show that the initial resistance to movement is negligible at all rates of loading but that some resistance was mobilised after a certain amount of displacement. They further conclude that the higher the rate of loading the larger is the resistance.

In contrast to the experimental work of Takahashi et al (2002) where a cylinder was pulled at different rates, the failure of the pile discussed here is more realistic. It failed due to instability and the rate diminishes from 19.2mm/s to 0.2mm/s, (at the level of pressure cells) as the pile progressively buckled by shearing the soil in front of it. It must be concluded that liquefied soil can generate some definite shear strength if it subjected to undrained monotonic shear strains.

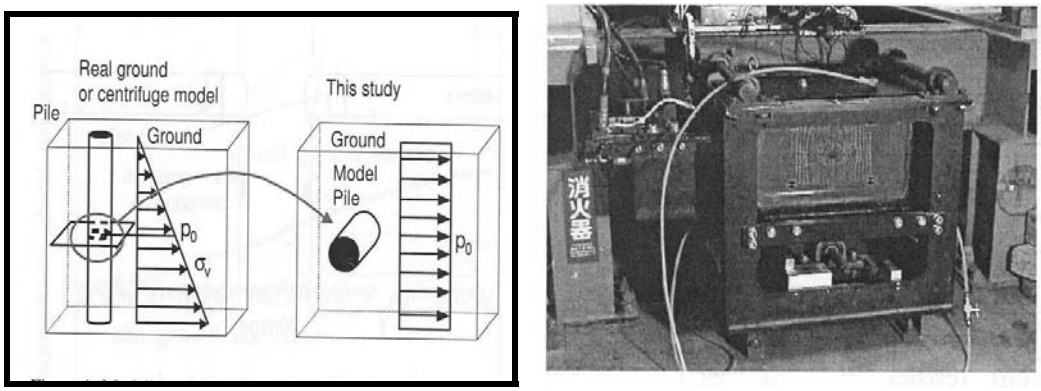

(a) (b)

Figure 6.4: Test set up of Takahashi et al (2002); (a): Modelling of pile at TIT, Japan; (b): Experimental set up

Takahashi et al. (2002) observed the deformation of the soil surrounding the cylinder just after the loading, shown in Figure 6.5. The black lines are the noodle markers placed vertically on the soil before the test. They also compared the deformation characteristics of the surrounding liquefied soil with and without ground vibrations. They measured and concluded that the lateral resistance for the case without vibration of the ground is remarkably larger than that for the case with vibration as also evident from the soil area influenced (Figure 6.5) in the respective cases. They note that the difference in the soil area influenced may directly affect the lateral resistance of the cylinder. The researchers linked this reduced resistance of the liquefied soil in the case of ground vibration to the instability of the contacts of the soil particles due to shaking.

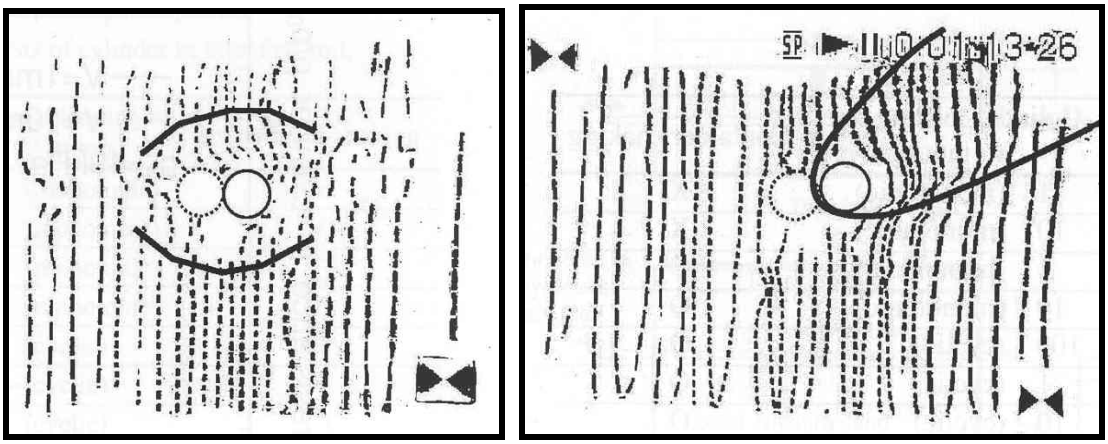

With ground vibration Without ground vibration

Figure 6.5: Deformation of the surrounding soil as the buried cylinder is pulled, Takahashi et al. (2002)

6.7 Pile-soil interaction during buckling

Sufficient information has been obtained from the centrifuge models to propose a hypothesis of pile-soil interaction during a buckling event. The pile begins to buckle when the front of zero effective stress reaches a critical depth H_C. This buckling instability will cause the pile to shear the soil adjacent to it, which will start offering temporary resistance. Figure 6.6 schematically shows the pile-soil interaction during the post-buckling period.

The soil element in front of the buckling pile, marked A in Figure 6.6, will be subjected to monotonic shearing in addition to the cyclic shearing due to earthquake. It is evident from the "V/k" ratio (i.e. the ratio of velocity of the pile to the permeability of the soil, which is of the order of 100's, see Figure 5.26) that the event is best looked upon as undrained. The resistance to the buckling pile is due to this "undrained strength of the soil" which is the strength when sheared at constant volume. It should be obvious from the definition that the stress path must follow the Critical State line.

In the q-p' plot shown in Figure 6.7, a soil element during the pre-buckling period, will start from some point in the q-p' plot, shown by X, and generate positive pore pressure due to the earthquake shaking. The stress path will progress towards the origin until it hits the "Phase Transformation" line. As discussed in chapter 2, the stress path will run up and down like a butterfly wing passing through or near the origin. At the same time, the pile length will progressively be unsupported by the soil grains, in top down fashion, until the critical depth is reached. As the critical depth is reached the pile starts to buckle. The behaviour of a soil element in front of the pile (marked A in Figure 6.6) can be described as similar to "Triaxial Extension" while the soil behind the pile (marked B in Figure 6.6) can be described as similar to "Triaxial Compression". Due to the mode shape of the pile the top-soil in the near field (marked 1 in Figure 6.6) will be sheared more than the bottom soil in the near field (marked 3 in Figure 6.6).

As discussed in section 2.2.2, the imposition of undrained monotonic shear strains (pile pushing the soil) in loose to medium dense sand at low effective stresses will lead to an attempt to dilate. The event being at constant volume will suppress this potential dilatancy by a negative increment of pore pressure in the locally sheared soil. This negative increment of pore pressure creates an increase in effective stress, which temporarily provides support to the buckling pile.

The pore fluid pressure in the sheared zone can drop to a maximum of -100kPa, which would correspond to the greatest possible effective stress increment during shearing. Beyond this value vapour bubbles tends to nucleate. In the stress path the soil element in front of the pile moves from Y to Z, Figure 6.7. This local reduction of pore pressure would induce a transient flow into

the sheared soil from the neighbouring "liquefied but not monotonically sheared soil" shown schematically in Figure 6.6. The lateral resistance of the liquefied soil would then decrease.

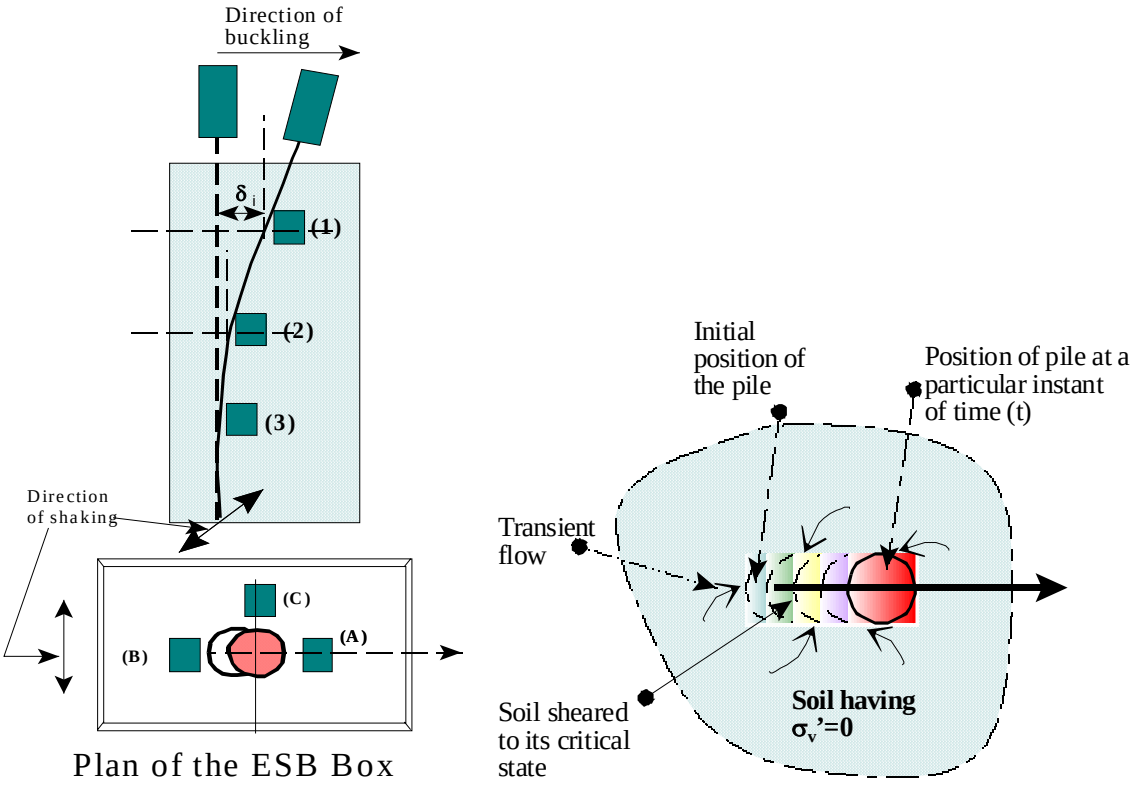

Figure 6.6: Pile-soil interaction during post-buckling

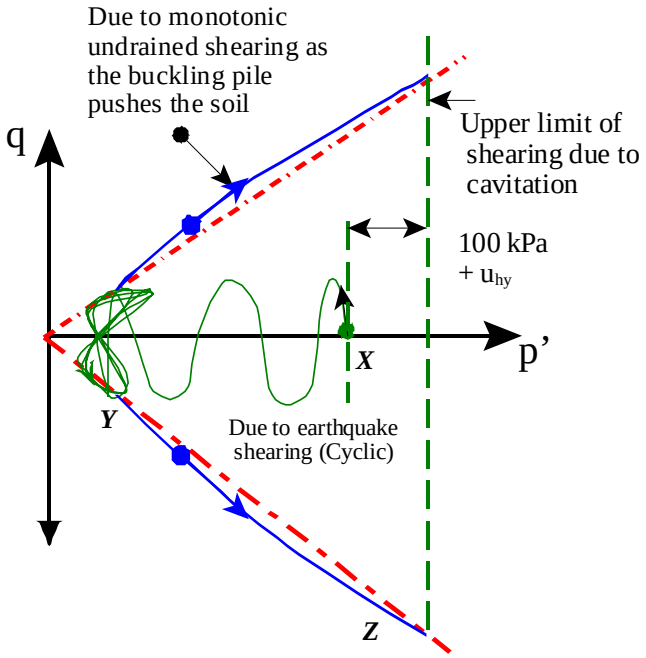

Figure 6.7: Stress path of a soil element close to the pile, where u_{hy} = hydrostatic pressure.

It is the upper part of a liquefiable sand layer that remains longest in a state of zero effective stress (Figure 5.18) due to upward hydraulic gradients, and it is the upper part of the pile which displaces most (Figure 5.22), and which can fully soften to zero shear strength the supporting soil adjacent to it. Ultimately, therefore, the upper part of the soil can be properly described as liquefied, in the true sense of the word in science or common language, according to the necessary conditions laid down in Schofield (1981) and Muhunthan and Schofield (2000) and mentioned in section 2.2.3. For the lower part of the pile, the resistance will increase as the pile shears the "*initially liquefied soil*" but not for a sufficient duration. This is due to development of negative pore pressure in the sheared soil which will induce transient flow from the neighbouring "*liquefied but not monotonically sheared*" soil. The buckling pile will also suffer increasing loss of bending stiffness due to plastic yielding, so the restraint necessary to hold it in equilibrium will also increase.

This imbalance between increasing bending moment created by displacement of pile cap, deteriorating bending stiffness of the pile and the reducing differential soil support along its length, creates a shallow plastic hinge which then leads to the dynamic collapse of the structure. The above phenomenon can be visualised by considering the simple experiment described in section 6.8. Section 6.9.2 discusses further on the formation of shallow hinge.

6.8 A simple experiment to demonstrate the failure of piles

The instability test described in Figure 3.2 is repeated with a hollow rigid tube partially jacketed around the slender columns as shown in Figure 6.8. A schematic view of the experiment is shown in Figure 6.9(a). It must be noted that the top part of the slender columns can move freely simulating the fully liquefied soil in the upper part of the liquefiable layer.

As discussed in section 6.6 the initial resistance to movement of pile in liquefied soil is negligible but some lateral resistance becomes mobilised after a certain amount of displacement. This behaviour can be visualised by the hollow co-axial rigid jacketed tube. In the light of the discussion of pile-soil interaction, this tube should be thought to expand its diameter gradually due to the softening of the soil induced by transient flow. Figure 6.9 (b) shows the mode shape of a failed pile in a centrifuge test, which is very similar to the mode shape of failures in the simple experiment.

The following conclusions can be drawn:

1. The buckling load or the critical load remain the same in experiments with or without the hollow rigid tube.
2. The location of the hinge is dependent on the post-buckling behaviour and depends on the resistance experienced by the buckling column after it became unstable.
3. The initial effective length of the pile cannot be estimated from the final buckled shape.

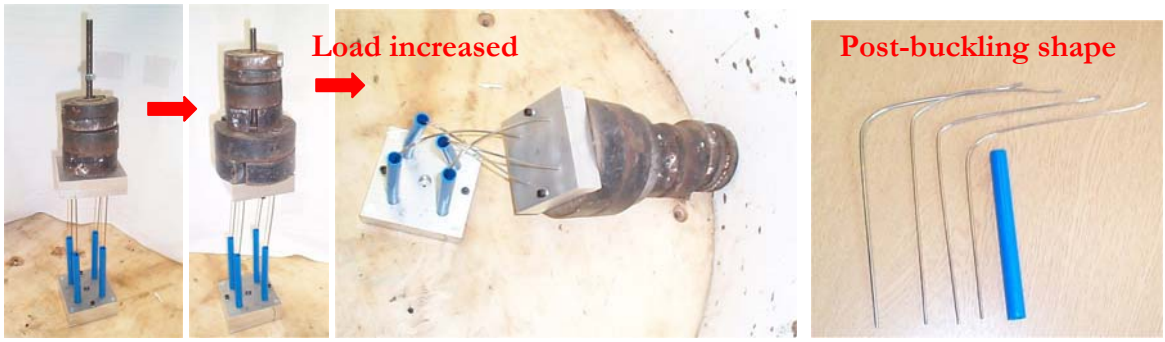

Figure 6.8: A simple experiment

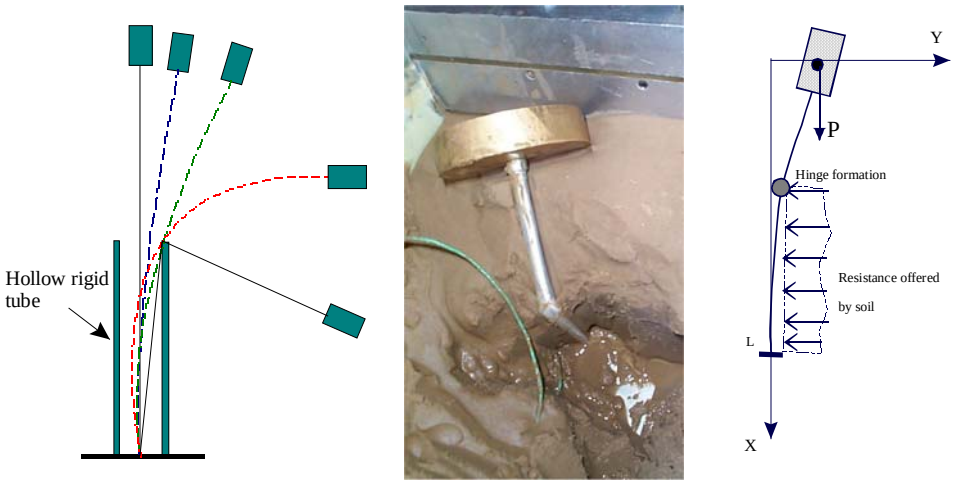

(a) Schematic of the simple experiment

(b) Pile 12 in the centrifuge

(c) Idealisation of pile buckling

Figure 6.9: Comparison of centrifuge models with simple models

6.9 Analytical approach for modelling the pile-soil interaction

The pile soil interaction can be subdivided into two phases, pre-buckling and post-buckling. It is clear from the earlier discussions that the pre-buckling behaviour is controlled by "Critical Load" and the stiffness degradation as soil liquefies. On the other hand, the post-buckling behaviour is controlled by "Critical State" soil mechanics. This section of the chapter will make an attempt to model analytically the pre-buckling as well as the post-buckling behaviour of pile.

6.9.1 Pre-buckling behaviour of pile

The basic differential equation for an axially loaded straight bar supported by an elastic medium can be expressed as shown by the equation 6.5, Hetenyi (1946).

$$EI\frac{d^4y}{dx^4} + P.\frac{d^2y}{dx^2} + k.y = 0 \qquad (6.5)$$ where

P=axial load.

EI = stiffness of the member (pile).

k= Modulus of foundation having units of ($F.L^{-2}$, F being the force and L is length). It is essentially soil reaction per unit length per unit deflection and is obtained by multiplying the modulus of subgrade reaction (η_h) with the diameter of the pile. Typical values of η_h can be obtained from API (1993), Tomlinson (1994). Table 6.3 quotes values of η_h from API (1993) Code.

Table 6.3: Values of η_h

Relative Density (%)	Value of η_h (MN/m^3)	
	Sand below the water table	Sand above the water table
40%	8	13
60%	24	42
80%	40	75

It may be shown that the general solution of equation 6.5 is of the form

$$y = C_1 e^{-\beta x}\cos(\alpha x) + C_2 e^{-\beta x}\sin(\alpha x) \qquad (6.6a)$$ where

C_1 and C_2 are the constants to be determined for a particular case of loading and boundary conditions and

$$\alpha = \sqrt{\left(\lambda^2 + \frac{P}{4EI}\right)} \qquad (6.6b)$$

$$\beta = \sqrt{\left(\lambda^2 - \frac{P}{4EI}\right)} \tag{6.6c}$$

$$\lambda = \sqrt[4]{\frac{k}{EI}} \tag{6.6d}$$

Substituting P=0 would lead to the special case of laterally loaded pile in the absence of axial load.

As soil liquefies, the stiffness of soil degrades and the value of k in equation 6.5 diminishes. The decrease in k is often related to pore pressure rise or shear strain in soil: Goh and O'Rourke (1999), Liyanapathirana and Poulos (2002), Haigh (2002). As k approaches zero, equation 6.5 reduces to Euler's buckling of struts.

The following two cases are considered here:

1. Fully embedded pile as shown in Figure 6.10(a). It represents the piles of the centrifuge tests. A specific example of failure of pile 12, described in chapter 5 (Table 5.2) is considered.
2. Partially exposed pile shown in Figure 6.10(b). This represents the piles of Showa Bridge shown in Figures 1.7, 1.8 and 3.3.

The derivation of the solutions can be seen in Hetenyi (1946). The results are quoted here.

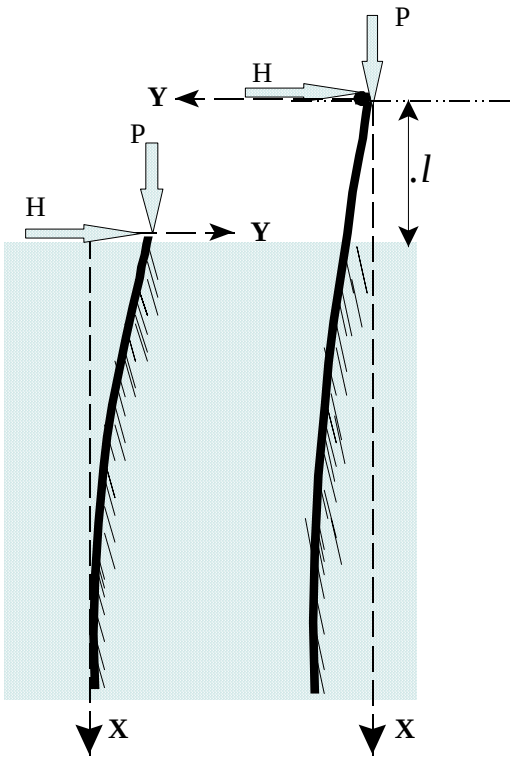

Figure 6.10 (a): Fully embedded pile, (b): Special case of Showa bridge pile configuration where part of the pile is exposed.

6.9.1.1 Fully embedded pile

The solution for deflection and bending moment for the case shown in Figure 6.10(a) is as follows:

Deflection

$$y = \frac{H}{\alpha.k}\left[\frac{2\lambda^2}{3\beta^2 - \alpha^2}\right]e^{-\beta x}\left[2\alpha\beta.\cos(\alpha x) + \left(\beta^2 - \alpha^2\right)\sin(\alpha x)\right] \tag{6.7}$$

Moment

$$M = \frac{H}{\alpha}\left[\frac{2\lambda^2}{3\beta^2 - \alpha^2}\right]e^{-\beta x}.\sin(\alpha x) \tag{6.8}$$

As can be seen from the expression for bending moment, there are two parts viz. a decaying function ($e^{-\beta x}$) and a sinusoidal function $\sin(\alpha x)$. Figure 6.11 show the plot of the above two functions for decreasing α and β values respectively. It becomes very obvious that as soil stiffness degrades the value of " k " diminishes and hence α and β also diminish following equations 6.6 (b&c). For moment estimation these two functions get multiplied and hence the point of maximum moment (X_M) will be close to the crest of the first sine wave given by equation 6.9.

$$\alpha.x = \frac{\pi}{2}, or X_M = \frac{\pi}{2.\alpha} = \frac{\pi}{2\sqrt{\left(\lambda^2 + \frac{P}{4EI}\right)}} \tag{6.9}$$

It should be noted that as soil liquefies, the value of λ decreases and the point of maximum bending moment shifts downwards.

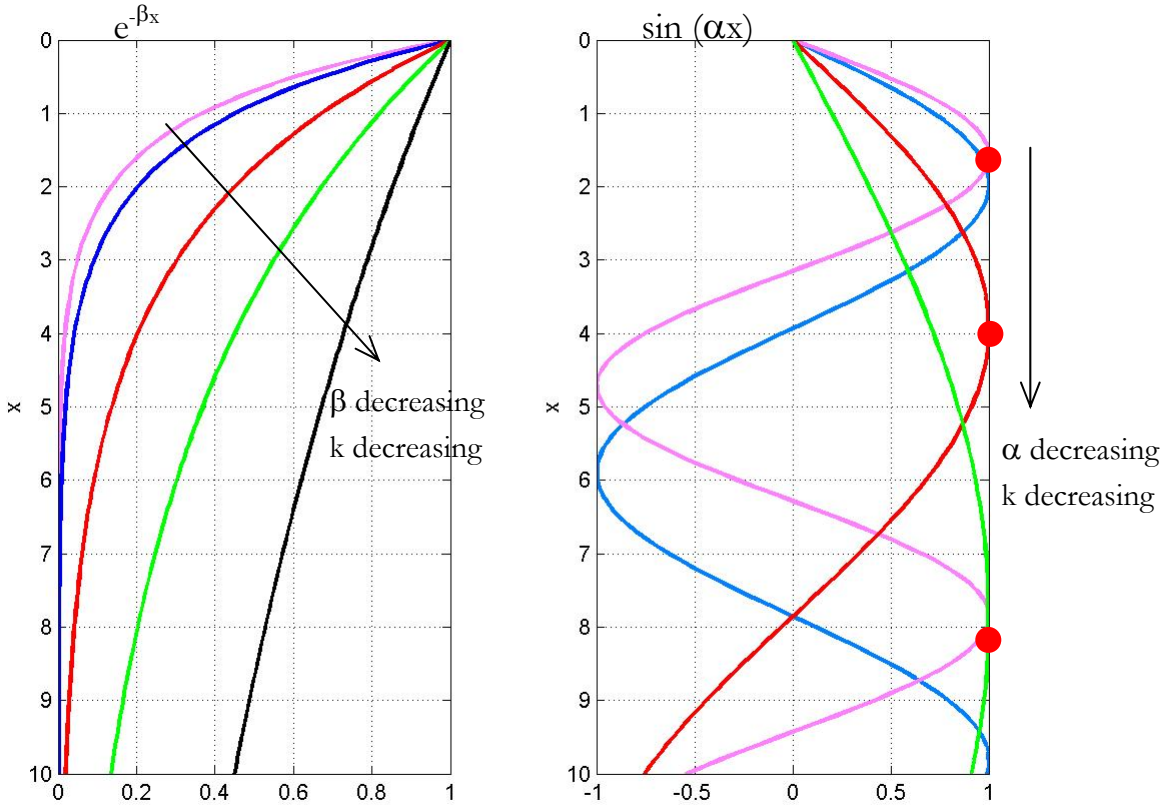

Figure 6.11: Plotting of two functions

In the case of Euler's buckling of struts, shown in Figures 3.1, 3.2, 5.14(c) and 5.15(b), the point of maximum bending moment is always at the bottom of the strut, and this is where the hinge forms. On the contrary, in the case of pile buckling, as can be observed from equation 6.9, the point of maximum bending moment may not necessarily be at the bottom of the pile. This agrees with the observations of the centrifuge test results that the hinge may form at shallow depths. The hinge will form where the moment induced in the section of the pile exceeds the plastic moment capacity (M_p).

Modelling of the failure of pile marked 12

As mentioned in chapter 5, this pile failed due to the combined action of inertia and axial load. The inertia load was measured using the accelerometer attached at the pile head. The analysis is carried out at prototype scale and the parameters used for the analysis are shown in Table 6.4.

Table 6.4: Parameters used for the analysis of failure of pile marked 12

Parameters	Values used in the analysis	Remarks
P (Axial load)	1.102MN	The values are calculated using the scaling laws for centrifuge tests, Table 4.1. The value of η_h is taken as 8 MN/m^2 for 40% relative density saturated sand, Table 6.3.
H (Inertial load)	0.045MN	
Length of the pile (L)	9.5m	
Diameter of the pile (D)	0.465m	
EI (Bending Stiffness)	48.6 MNm^2	
M_p (Plastic moment)	1021kNm	
k (Soil stiffness prior to earthquake)	3.72MN/m^2 (From API Code)	

The stiffness of the soil (k) was reduced from 3.72MN/m^2 in steps to 0.033MN/m^2 i.e. 0.9% soil stiffness. The bending moments and the deflections are computed in each step and plotted in Figure 6.12. It is assumed that the horizontal load (H) is static and is always acting at the pile head in one direction. However in reality the load is dynamic and is usually of the form H.sin(wt).

From Figure 6.12 it must particularly be observed that as the stiffness value reached 2% of the soil stiffness in un-liquefied condition, a small decrease in soil stiffness caused instability in the pile, the deflection amplified by almost 300%. The analysis predicts that the hinge should form at 7m depth i.e. where the moment exceeds M_p. Actually the hinge formed at 5m from the point of application of the load, Figure 5.31.

The analysis however does not reflect the fact that the liquefaction front travels top-down. It assumes that the entire soil as a whole gradually softens. It must however be appreciated that the results show that an initially straight pile can buckle under the action of axial load if the surrounding soil liquefies in an earthquake. Large lateral loads are not needed.

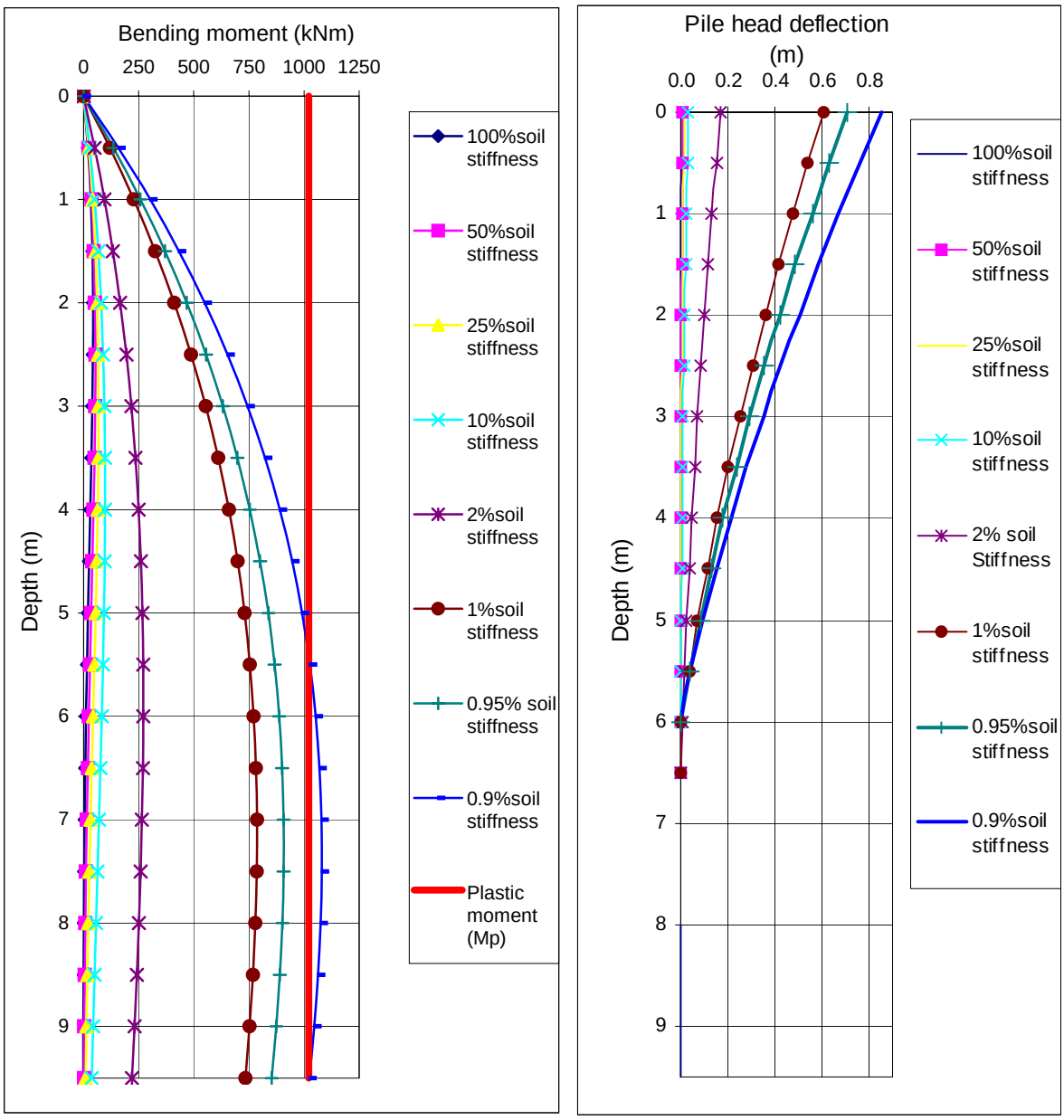

Figure 6.12: Bending moment and deflection for Pile marked 12

6.9.1.2 Partially exposed pile, a special case of Showa Bridge piles

The solution for deflection and bending moment for the pile as shown in Figure 6.10(b) is given by equations 6.10 and 6.11, Hetenyi (1946). The bending moment and deflection are functions of H, P, k, EI, *l* (cantilever length).

Moment

$$M_x = A.P.\sin(c.x) \qquad (6.10)$$

Deflection

$$y = A.\sin(c.x) - \left(\frac{H}{P}\right)x \tag{6.11a}$$

where

$$c = \sqrt{\frac{P}{EI}} \tag{6.11b}$$

$$A = \frac{H\left[\frac{EI}{P}(3\beta^2 - \alpha^2) + 1\right]}{EI(3\beta^2 - \alpha^2)c.\cos(c.l) - 2.P.\beta.\sin(c.l)} \tag{6.11c}$$

The example of the piles of Showa Bridge is considered to demonstrate the effects of axial load as soil liquefies. This example is chosen as this bridge collapsed just one month after construction, and had steel tubular piles. This ensures less uncertainty of material strength, as degradation of piles due to corrosion is not expected. The shape of the pile after failure is also known and is shown in Figure 2.16. Moreover this case history is well documented by Fukuoka (1966) and soil tests were carried out after the earthquake. The design data used for the analysis is shown below in Table 6.5 and the properties of the pile along the depth are shown in Table 6.6.

Table 6.5: Parameters used for the analysis of failure of piles Showa Bridge

Parameters	**Values used in the analysis**	**Remarks**
P (Axial load)	0.96 MN	P is the allowable load, Section 3.2.1 H is 5% of axial load (assumed)
H (Inertial load)	0.05MN	
Length of the pile (L)	25m	
Diameter of the pile (D)	0.609m	
k (Soil stiffness prior to earthquake)	6 MN/m^2 (From Fukuoka, 1966)	
Cantilever length (l)	9m	

Table 6.6: Properties of the pile section of Showa Bridge

Depth	**Material and section**	**Int. dia.**	**Ext. dia**	**EI($MN.m^2$)**	**Plastic moment (kNm)**
0m-12m	Steel tubular pile	577mm	609mm	275	5627
12m-25m	Steel tubular pile	591mm	609mm	160	1620

It must be noted from Table 6.6 that the plastic moment of the section is reduced by a factor of 3.5 at 12m depth.

Soil properties at the Bridge site

Soil tests were carried out after the earthquake in the bridge site, Fukuoka (1966). The top 10m of soil had a void ratio of 1.23 and at 11m it is 0.85. The void ratio decreased to 0.56 at 13m depth. The SPT value of the soil along the depth is plotted in Figure 3.3. It is assumed that the top 10m is liquefiable soil and the value for η_h is 10MN/m^3, Fukuoka (1966), which is comparable with the recommendations of the API (1993) code. API (1993) recommends a value of η_h as 8MN/m^3 for 40% relative density medium-loose sands.

The value of k is decreased from 100% to 5% and the bending moments and deflections are computed and plotted in Figures 6.13 and 6.14 respectively.

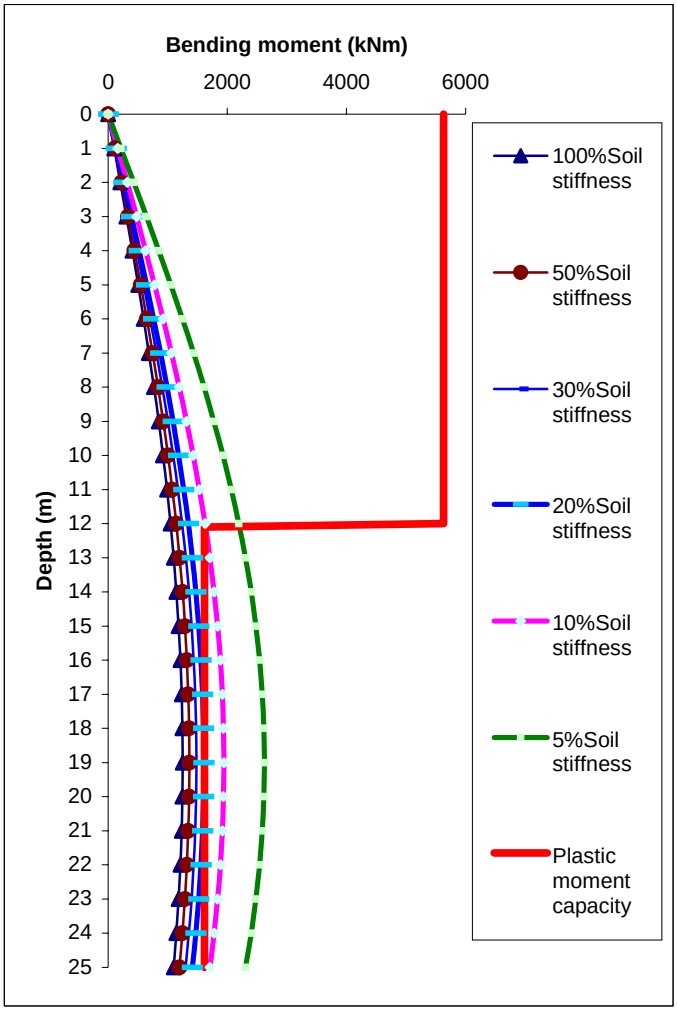

Figure 6.13: Bending moment of one of the piles of the Showa Bridge for degrading soil stiffness.

It may be noted from Figure 6.13 that as the value of soil stiffness degrades the bending moment in the pile increases. The point of maximum moment also shifts downward along the depth as mentioned earlier. At 20% stiffness the bending moment exceeds the plastic moment capacity and this signifies yield of the section. At this stage the pile head deflection is 0.6m. The mode shape of the buckling pile is quite similar to the shape of the pile after failure as shown in Figure 2.16 highlighted as "original position".

The above example of the failure of piles of Showa Bridge validate the results of centrifuge tests that axial load, combined with a slight amount of imperfection or lateral load, can cause a pile to fail as the soil surrounding the pile liquefies in an earthquake. There is no need to have lateral spreading and the pile can fail before lateral spreading starts.

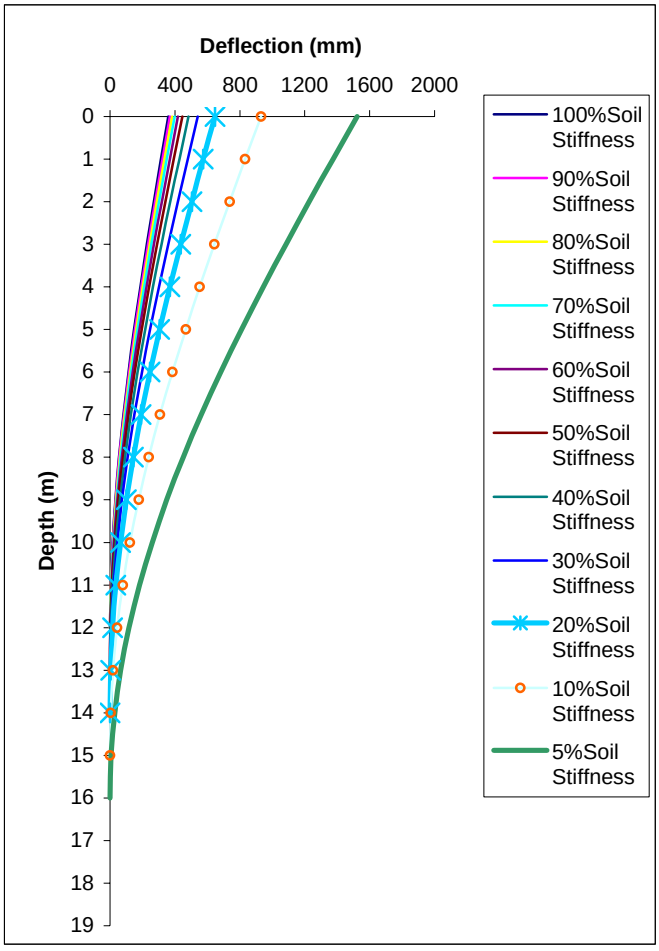

Figure 6.14: Deflection of the pile due to stiffness degradation of the surrounding soil

In the above example, stiffness variation with depth in the soil layer, and relating pore pressure rises with the percentage of stiffness degradation, are not attempted. The central aim was to establish the importance of the effect of axial load as soil liquefies which is currently missing in

all codes of practice. It may be concluded that the part of the pile passing through liquefying soil should be checked against Euler's buckling.

6.9.2 Post buckling behaviour of pile

This section makes an attempt to model analytically the pile-soil interaction after the pile has buckled and during shearing of the soil next to it. Prediction of some of the results of the centrifuge tests is also attempted, for example the point of hinge formation or increase in effective stress in the sheared zone as discussed in section 6.7.

Figure 6.15 shows the free body diagram of a buckling pile in liquefied soil. It will be assumed that the undrained resistance of the liquefied soil holds the pile in quasi-static equilibrium until the transient flow feeds the dilation of the shearing soil and reduces the resistance. The pile then moves to a new equilibrium position.

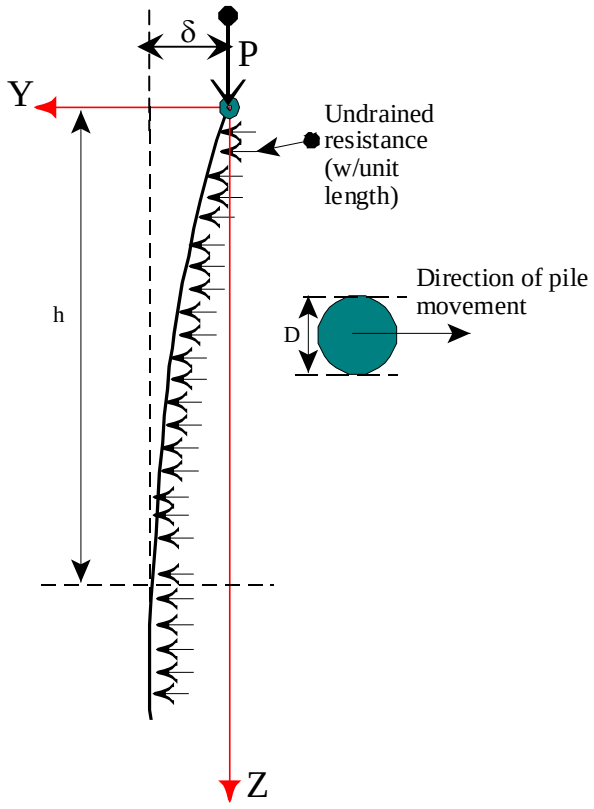

Figure 6.15: Free body diagram of a buckling pile.

In this analysis, dynamic effects are not taken into consideration. The mobilisable undrained resistance of the soil (w) is assumed to be constant with depth and is the difference in pressure between front and back of the pile in the direction of buckling.

From the moment equilibrium at any depth z, the differential equation 6.12a is obtained

$$EI\frac{d^2y}{dz^2} = -\left(P.y - w.\frac{z^2}{2}\right) \quad (6.12a)$$

Rearranging equation 6.12a gives the form 6.12b

$$\frac{d^2y}{dz^2} + \left(\frac{P}{EI}\right).y - \frac{w}{2EI}z^2 = 0 \quad (6.12b)$$

The general solution of equation 6.12b is given by equation 6.13

$$y = A.\sin(\lambda z + B.\cos(\lambda z) + (\frac{w}{2P}).z^2 - \left(\frac{wEI}{P^2}\right) \quad (6.13), \text{ where}$$

$$\lambda = \sqrt{\frac{P}{EI}} \quad (6.14)$$

Applying the following boundary conditions

1. At z = 0; the relative pile head displacement is zero i.e. y = 0
2. At z = h; the slope is zero i.e. $\left(\frac{dy}{dz}\right) = 0$,

The general expression for deflection is obtained (6.15)

$$y = \frac{w}{P.\lambda^2}\left[\left(\tan(\lambda h) - \frac{\lambda h}{\cos(\lambda h)}\right)\sin(\lambda z) + \cos(\lambda z) + \frac{(\lambda z)^2}{2} - 1\right] \quad (6.15)$$

The above equation is only stable for $\lambda h < (\pi/2)$ i.e. P less than P_{cr} (Critical load). Making an engineering assumption that curvature is zero at z = h, provides an estimate of the depth h. A similar type of approximation is used by Hobbs (1985) while studying the buckling of seabed pipelines.

Imposing the condition, at z = h, $\frac{d^2y}{dz^2} = 0$; the following condition, equation 6.16, is obtained

$$\tan(\frac{\lambda h}{2}) = \lambda h \quad (6.16)$$

The first root that satisfies equation 6.16, is (λh) = 2.325 which will give the expression for h.

$$h = 2.325\sqrt{\frac{EI}{P}} \quad (6.17)$$

The general equations for displacements and moments are given by equation 6.18 and 6.19 respectively.

Deflection

$$y = \frac{w}{P.\lambda^2}\left[2.33\sin(\lambda z) + \cos(\lambda z) + \frac{(\lambda z)^2}{2} - 1\right] \quad (6.18)$$

Moment

$$M_z = \frac{w}{\lambda^2}\left[2.33\sin(\lambda z) + \cos(\lambda z) - 1\right] \quad (6.19)$$

Using the above set of equation, the pile head deflection will be estimated:

1. **Pile head deflection (δ)**:

Substituting z = h, the deflection (y) will reveal the pile head deflection (δ) given by equation 6.20;

$$\delta = \frac{2.72w}{P.\lambda^2} \quad (6.20) \text{ giving}$$

$$w = \frac{0.36P^2\delta}{EI} \quad (6.20a)$$

From the above expression it must be concluded that as the pile deflects, more resistance has to be generated by the soil to keep the pile is quasi-equilibrium. This is in agreement with the pore pressure data of the centrifuge tests, Figure 5.23, where additional sharper downward spikes was noticed at the end of each earthquake cycle, representing the generation of negative pore pressure compared to its surrounding soil.

2. **Maximum moment or the point of hinge formation (Z_h)**:

For maximum moment; $\frac{dM_z}{dz} = 0$; which gives the following expression

$$Z_h = 1.165\sqrt{\frac{EI}{P}} \quad (6.21)$$

Comparing with equation 6.17 it is evident that the point of hinge formation will not be at the bottom (i.e. z = h) and will approximately be at half the value of h.

6.9.2.1 Comparison of the prediction of hinge formation for the piles in the centrifuge tests

Piles 7, 8 and 9 were subjected only to axial load. Table 6.7 compares the location of hinge formation with the predicted location based on equation 6.21. Figure 6.16 shows the location of the hinge formation for the three piles. It may be concluded that the analysis reasonably predicts the location of hinge formation. Assumption of non-uniform undrained resistance may give a more accurate prediction but it is beyond the scope of the present work.

Table 6.7: Comparison of the prediction with the actual hinge formation

Pile ID	**P**	**Depth of zero slope (h)**	**Z_h (Predicted hinge location)**	**Actual hinge location**
Pile#7 EI=7.77x10^6 Nmm^2	610N	261mm	131mm	80mm from the C.G of the block.
Pile#8 EI=7.77x10^6 Nmm^2	872N	220mm	110mm	83mm from the C.G of the block.
Pile#10 EI=7.77x10^6 Nmm^2	735N	239mm	120mm	118mm from the C.G of the block

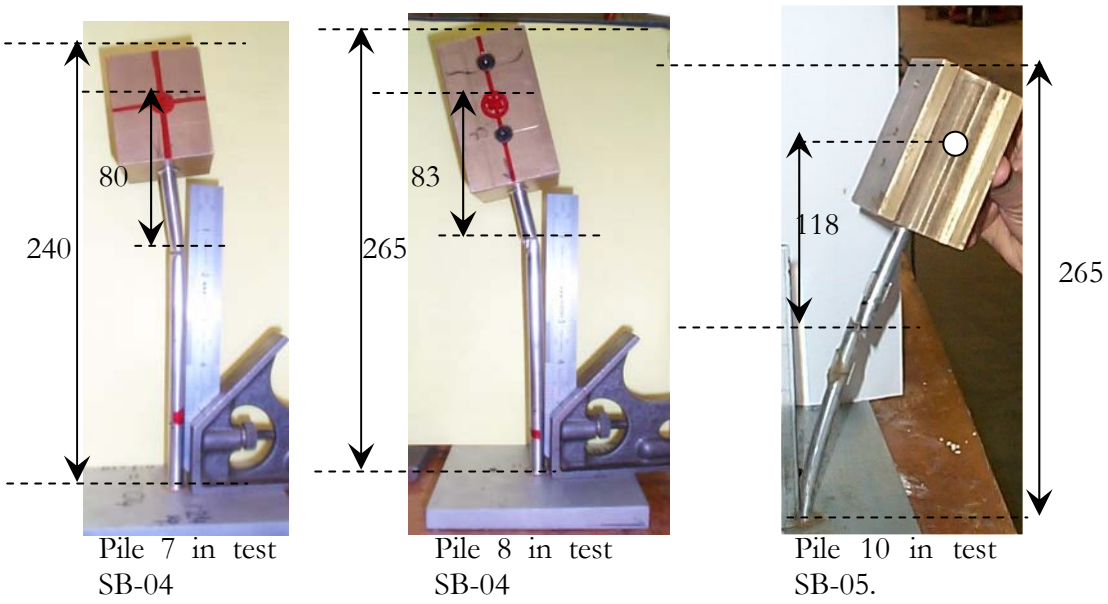

Pile 7 in test SB-04 Pile 8 in test SB-04 Pile 10 in test SB-05.

Figure 6.16: Location of hinge formation in the tests.

6.9.2.2 Increase in effective stress in the sheared soil

The undrained resistance of the soil is represented by w (Figure 6.15) and is the difference in soil reaction due to the horizontal motion of the pile in the liquefied soil. It is assumed that the soil maintains the pile in quasi-static equilibrium and thereby reaches a limiting condition. The stress path of the shearing soil element moves along the critical state line. At each position of the pile, there is a unique value of q in the q-p' plot (Figure 6.7) and it may be reasonable to assign a single

deviatoric strain (ε_q) in the soil in the zone of plastic deformation. The soil in front of the pile will form an "undrained mechanism" as shown in Figure 6.17.

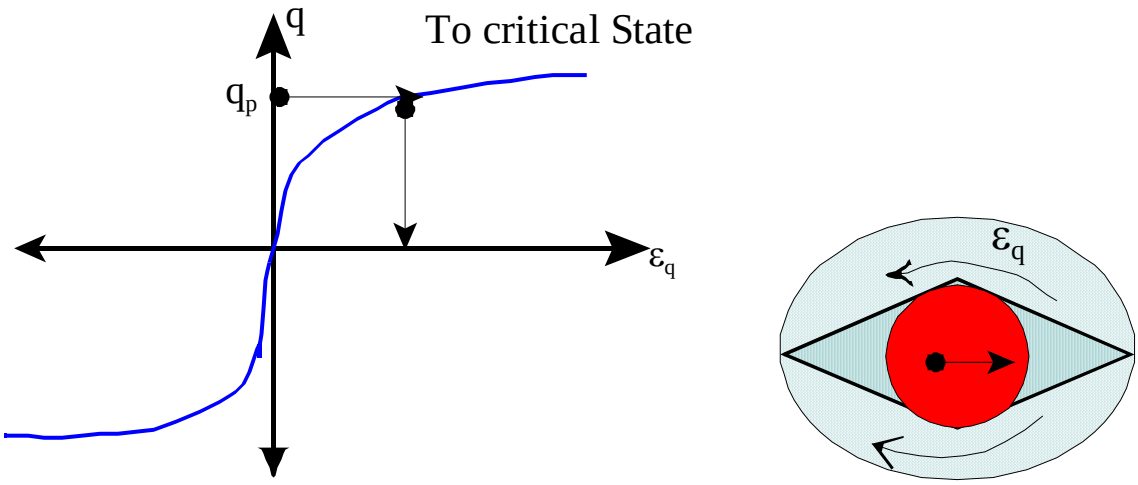

Figure 6.17: Undrained mechanism surrounding the pile

If the shear stress induced in the soil is denoted by τ_p, the ultimate resistance of the soil (w) can be approximated by equation 6.22, following Randolph and Houlsby (1984).

$$w = 10.\tau_p.D \qquad (6.22)$$

Combining equations 6.20 and 6.22 gives an expression for the limiting shear stress τ_p acting on the pile.

$$\tau_p = \frac{P.\lambda^2}{27.2D}\delta \qquad (6.23)$$

The effective stress or the negative excess pore pressure generated can be estimated using equation 6.24.

$$p' = \frac{\tau_p}{\sin\varphi_{PTL}} \qquad (6.24), \text{ where}$$

ϕ_{PTL} is the angle of "Phase Transformation".

Specific example of Pile 8

For Pile 8 near field pore pressures were measured and are shown in Figure 5.23. The pile head moved by 20mm before the pile head mass rested on the ground. The data required for the prediction is shown in Table 6.8.

Table 6.8: Prediction of negative pore pressure in near field for pile 8

Parameters	Value
P (axial load)	872N
λ (Equation 6.14)	0.0106 (1/mm)
D (outside diameter)	9.3mm
ϕ_{PTL}	32 degrees

$\tau_p = 0.275\,\delta$, in kPa, where δ is in mm, following equation 6.23

$p' = \dfrac{\tau_p}{\sin\varphi_{PTL}} = 0.52\delta$ in kPa; where δ is in mm, following equation 6.24

For 20mm movement, it is expected to have a mean effective stress increase of 10 kPa. This should also be the amount of negative excess pore pressure to be generated in the locally sheared soil relative to the liquefied far field. PPT records show that the suction generated was of the order of 10 to15kPa (see Figure 5.23).

6.10 Summary

The failure of pile-supported structures during earthquakes in liquefiable level ground may be decomposed into three phases:

[1] Soil and pile response to earthquakes

[2] Pile response to soil stiffness degradation

[3] Soil response to pile buckling behaviour

The first phase is the generation of excess pore pressure in the soil whereby the effective stress comes to oscillate near zero. The piled structure also vibrates. In the second phase, the piled structure may become unstable, if the slenderness ratio of piles exceeds a critical limit depending on the axial load and the pile material. In other words, the response would dictate whether the pile would buckle and push the soil monotonically. In the third phase, if the pile buckles, it would shear the initially liquefied soil; there would be local reduction of pore fluid pressure inducing a transient flow.

Seismic pile-soil interaction in liquefiable soil is a very complex phenomenon involving different mechanisms and physical processes. All the processes are highly non-linear. For example,

buckling is itself non-linear and earthquake perturbations makes it even more non-linear. The pre-buckling behaviour of pile is governed by the "Euler's elastic critical load" and the post-buckling behaviour is controlled by "Critical State" soil mechanics. The pile-soil interaction in level ground can be described as a combination of two critical phenomena and transient flow.

It has been shown that liquefied soil cannot prevent the initiation of buckling but will dictate the location of a hinge by offering lateral resistance to the buckling pile. The quantification of lateral resistance is dependent on various factors. They include:

1. Relative density of soil and type of soil i.e. grain type and presence of fines.
2. Angle of Phase transformation or ϕ_{PTL}
3. Angle of dilatancy (ψ)
4. Soil permeability (k)
5. Excess pore pressure generation
6. Earthquake shaking characteristics i.e. frequency, duration and PGA
7. Soil layering
8. Pile stiffness EI
9. Axial load in the pile (P)
10. Loading rate or the velocity of buckling which is dependent on the C.G of the superstructure
11. Group effect of the piles
12. Pile installation method.

However, from the design point of view, the quantification of lateral resistance is irrelevant because of the fact that a piled structure should not become unstable even at full liquefaction. As discussed in chapter 2, the present design code does not ensure stability of piled structures during full liquefaction. A design method is proposed in chapter 7 to take into account the buckling effect.